
ORCNET: A CONTEXT-BASED NETWORK TO SIMULTANEOUSLY SEGMENT THE OCULAR REGION COMPONENTS

Diego Rafael Lucio, Luiz A. Zanlorensi
DINF
Federal University of Paraná
Curitiba, Paraná, Brazil
{drlucio, lazjunior}@inf.ufpr.br

Yandre Maldonado e Gomes da Costa
PCC/DIN
State University of Maringá
Maringá, Paraná, Brazil
yandre@din.uem.br

David Menotti
DINF
Federal University of Paraná
Curitiba, Paraná, Brazil
menotti@inf.ufpr.br

ABSTRACT

Accurate extraction of the Region of Interest is critical for successful ocular region-based biometrics. In this direction, we propose a new context-based segmentation approach, entitled Ocular Region Context Network (ORCNet), introducing a specific loss function, i.e., the Punish Context Loss (PC-Loss). The PC-Loss punishes the segmentation losses of a network by using a percentage difference value between the ground truth and the segmented masks. We obtain the percentage difference by taking into account Biederman’s semantic relationship concepts, in which we use three contexts (semantic, spatial, and scale) to evaluate the relationships of the objects in an image. Our proposal achieved promising results in the evaluated scenarios — iris, sclera, and ALL (iris + sclera) segmentations —, outperforming the literature baseline techniques. The ORCNet with ResNet-152 outperforms the best baseline (EncNet with ResNet-152) on average by 2.27%, 28.26% and 6.43% in terms of F-Score, Error Rate and Intersection Over Union, respectively. We also provide (for research purposes) 3,191 manually labeled masks for the MICHE-I database, as another contribution of our work.

1 Introduction

Recently, the interest in the use of biometrics to automatically verify or identify a person has increased. The fact that the biometric features (physical and behavioral) of a person cannot be lost or forgotten, as it can happen with other means of identification, such as passwords or identity cards, justifies this growth [1, 2].

Several physical characteristics of the human body, such as fingerprints, face, voice, and ocular region components, can be used as input for biometric systems. Among the previously mentioned physical attributes, the ocular region components have high discriminative power and, due to this fact, these components are an excellent choice to develop a non-invasive user identification system [3, 4, 5, 6, 7, 8, 9].

Fig. 2 shows the iris, pupil, sclera, and the periocular region, which are the most commonly employed ocular region components in biometrics. According to Bowyer et al. [2], the pupil region is the central portion of the eye and it is generally darker than the iris. However, in some cases, there may be specular reflexes and cataracts, possibly making it clearer. The iris is a colored ring composed of tissue placed around the pupil through which light enters the eye. The sclera is a white region of connective tissue and blood vessels that surrounds the iris. For the periocular region,

there is no standard definition in the literature regarding the location of the Region of Interest (RoI). Some researchers considered the center of the iris as a reference point and calculated the width and the height of RoI as $6\times$ and $4\times$ the radius of the iris, respectively [10, 11, 12]. In contrast, Padole and Proença [13] proposed the use of the eyes corners as the reference point to calculate the RoI as they are less affected by gaze, pose variation and occlusion.

Among the previously mentioned ocular region components, the iris presents one of the most accurate results, since it has a sufficiently complex texture patterns that can be used on the identification task [8, 14, 15, 16]. However, in the last years, the experiments carried out using the sclera and the entire ocular region have also presented promising results on biometric tasks [17, 18, 19, 20, 21].

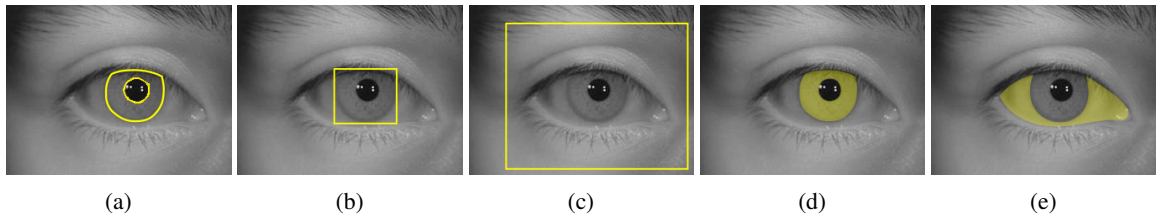


Figure 1: Detection and segmentation samples: (a) circular iris detection [22]; (b) rectangular iris detection [23]; (c) eye detection [24]; (d) iris segmentation [25]; (e) sclera segmentation [26];

As stated previously, the ocular region components can be employed as input to biometrics, once these components present a high level of differentiation between users [6, 27, 19, 20, 21]. However, the images need to be submitted to a preprocessing stage to extract the RoI. The preprocessing stage has great importance in a biometric system, because if the RoI extraction is erroneously performed, the system effectiveness may be injured (patterns can be removed and/or introduced into the RoI) [26, 28].

Taking into account the importance of the preprocessing stage in the ocular region based biometrics, many different approaches were proposed to solve the RoI extraction problem. The most common approaches employed to solve the RoI extraction problem in the ocular region can be seen in ground truth samples present in Fig. 1. Fig. 1(a) presents one of the first attempts of iris segmentation, where the RoI was delimited by the internal and external contours of the iris [29, 22]. Fig. 1(b) and Fig. 1(c) present the delimitation approaches employed to detect the iris and eye respectively [23, 24]. Fig. 1(d) and Fig. 1(e) present the delimitation approaches employed to segment the iris and sclera respectively [25, 26].

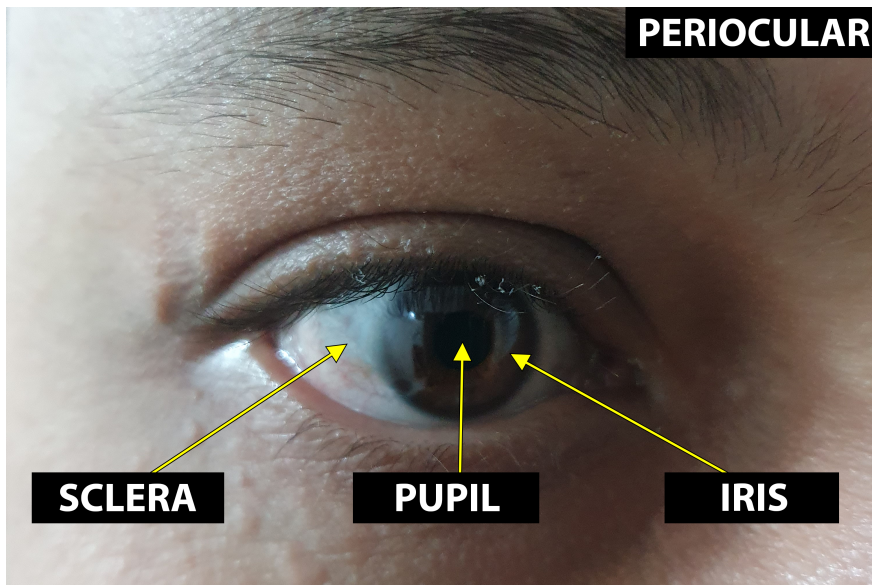


Figure 2: Ocular region components employed in biometric systems.

The most commonly employed preprocessing steps are: contour detection [29], Hough transform [30], active contours [31, 32], integro-differential equation [33], Maximum Radial Suppression (MRS) [34], Markovian Texture Models (MTMs) [35], Convolutional Neural Networks (CNNs) [26, 25, 36, 37, 24, 38].

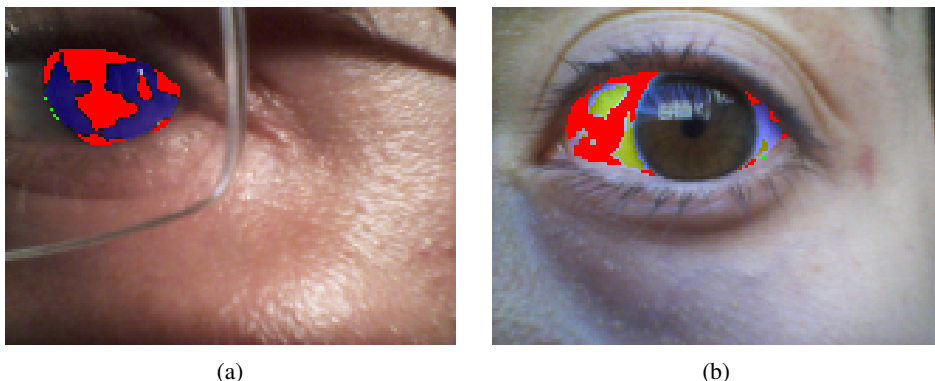


Figure 3: Samples of bad iris and sclera segmentation in experiments using Fully Convolutional Networks (FCNs). The green regions in images show wrong segmented regions, while the red regions show not segmented regions.

Besides the high number of component-based preprocessing segmentation approaches, none of them works correctly in specific scenarios, such as in non-controlled environments. Performing an analysis of why the segmentation of the presented images in Fig. 3 is so bad, it was found that this issue occurs because the FCN approach is not able to deal very well with blur and specular highlights present in the images.

The use of CNNs to extract the RoIs, taking into account context information is a promising approach, due to: (i) the available segmentation approaches do not work correctly in some scenarios; (ii) the context in which the ROI extraction is performed is not used by currently available approaches; (iii) the capabilities of decision power presented by the deep learning approaches. We can understand how the objects in a scene are related using contextual information.

We evaluate three different types of context in order to understand the objects relationship, i.e., semantic (*evaluates the likelihood of an object to be found in some scenes but not in others*), spatial (*evaluates the placement among objects in a scene*) and scale (*evaluates the size ratio among the different classes of objects in a scene*).

Thus, the main question addressed in this work is “Can we improve the ROI extractor in ocular region components taking into account the context information present in an image?”

Aiming to answer this question, we propose the Ocular Region Context Network (ORCNet) as a new segmentation approach to simultaneously segment the sclera and iris using contextual information. The proposed approach combines the Context Encoding Network (EncNet) with the main contribution of this work, the Punish Context Loss (PC-Loss). The PC-Loss consists of punishing the segmentation *Losses* of a network by using a percentage difference value between the ground truth and the segmented masks. We obtain the percentage difference by taking into account Biederman’s semantic relationship concepts, in which we use three contexts (semantic, spatial, and scale) to evaluate the relationships of the objects in an image.

The main contributions of this paper are: (i) the PC-Loss that consists into punishing the segmentation *Loss* of the network by using a percentage value obtained, taking into account the Biederman’s[39] semantic relationships concepts, (ii) 3,191 new manually labeled masks of the MICHE-I dataset (sample of iris and sclera image can be seen in Fig. 4), that is one of the most known datasets in the biometrics scenario, (iii) the novel ORCNet architecture that combines the *Context Encoding Module* proposed in [40] and the PC-Loss punishing approach presented in this work.

The remainder of this work is organized as follows: we review related works in Section 2. In Section 3, there is a description of the proposed methodology to perform iris and sclera segmentation using the contextual information of the image. Section 4 presents the datasets, evaluation protocol and baselines used in the experiments. We report and discuss the results in Section 5. We state our conclusions in Section 6.

2 Related Works

In this section, we review several approaches for ocular region components extraction. More specifically, we discuss works related to segmentation in Section 2.1, and in Section 2.2, we present works in which the contextual relationship among the elements present in the image are explored.

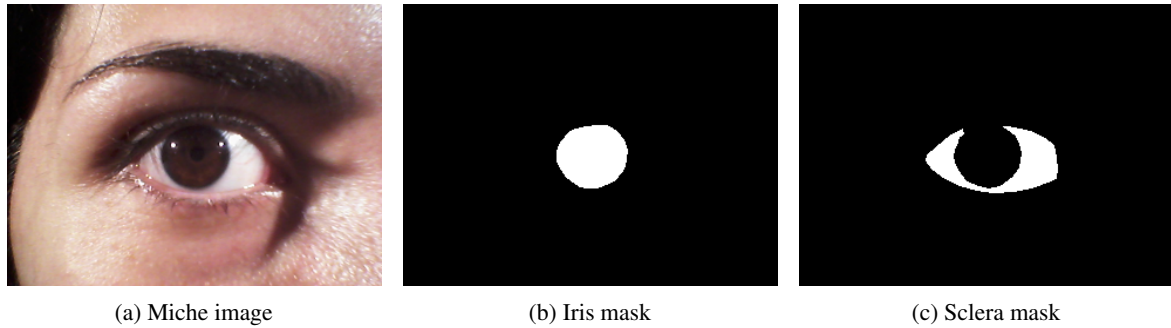


Figura 4: Sample of iris and sclera masks for an image

2.1 Segmentation

As previously stated, segmentation has great importance in the biometric systems. This importance comes from the fact that an incorrect extraction of the RoI can affect the effectiveness of the whole system.

Inspired by the excellent results obtained by using Convolutional Neural Network (CNN) approach in computer vision domain, many authors have proposed CNN based approaches to extract the ocular region components [37, 25, 41, 42, 43].

Liu et al. [37] was one of the first authors to propose the use of CNN to iris segmentation. They proposed two new approaches called Hierarchical Convolutional Neural Networks (HCNNs) and Multi-scale Fully Convolutional Networks (MFCNs). Performing a dense prediction of the pixels using sliding windows, merging shallow and deep layers, they achieved 0.90% and 0.59% Error Rates (ERs) on the UBIRIS V2 and CASIA-IrisV4-Distance [44] databases.

Bezerra et al. [25] presented a FCN-based approach, and achieved state-of-the-art results on the employed databases, i.e., BioSec [45], CASIA-IrisV3-Interval, CASIA-IrisV4-Thousand, IIIT-Delhi Contact Lens Iris (IIIT-D CLD)[46], NICE.I [47], CROSS-EYED [48] and MICHE-I [49], obtaining ERs of 0.58%, 0.55%, 1.25%, 0.72%, 2.67%, 1.12%, and 1.90%, respectively.

Osorio-Roig et al. [41], similarly to Bezerra et al. [25], have also presented a FCN approach to iris segmentation. In the proposed approach, the authors employed a multi-class training, however, only the iris segmentation was evaluated. To evaluate the proposed approach, the NICE-I competition protocol was employed in two well-know iris datasets, MobbIO [50] and NICE-I, obtaining ERs of 2.46% and 1.13%, respectively.

Zhao and Kumar [51] proposed the UniNet.v2, a new iris segmentation approach, and just like Osorio-Roig et al. [41] used the NICE-I competition protocol to evaluate the obtained results. The datasets employed to evaluate the UniNet.v2 are: ND-Iris-040, CASIA-Iris-Distance and IITD, obtaining ERs of 1.68%, 0.67%, and 5.34%, respectively.

Despite the consolidation of the iris as a biometric resource, other elements that compose the ocular region have started to arouse the interest of the researchers. Besides the iris, the sclera was one of the first ocular region components to attract the attention of the researchers, once the biometric systems based on such trait achieved interesting results [21]. Some works were proposed [26, 42, 52] taking into account the good results on sclera based biometrics and the need for a proper delimitation of the RoI, as well as in the iris-based biometrics.

Lucio et al. [26] proposed two new approaches to sclera segmentation. The first one is based on the Generative Adversarial Networks (GANs) [53], and the second approach is based on Fully Convolutional Networks (FCNs) [54]. The best results were obtained using the FCN approach achieving F-Score values of 87.48%, 88.32%, 88.12%, 87.80% and 87.94% on the UBIRIS V2, MICHE-I, MICHE-GS4, MICHE-IP5, and MICHE-GT2 databases, respectively.

Rot et al. [42] proposed a multi-class segmentation approach based in the SegNet to segment simultaneously the sclera and another components from the periocular region (iris, pupil, periocular, eyelashes and canthus). The authors employed the Multi-Angle Sclera Database (MASD) in the evaluation of the proposed approach, obtaining F-Score vales of 91.00%, 91.00%, 85.00%, 90.00%, 63.00% and 53.00% on the iris, sclera, pupil, periocular, eyelashes and canthus regions, respectively.

Wang et al [52] presented a new sclera segmentation approach based in the U-Net, and achieved F-Score vales of 91.43%, 89.54%, 90.45%, 89.28% and 89.34% on the UBIRIS V2, MICHE-I, MICHE-GS4, MICHE-IP5, and MICHE-GT2 databases, respectively.

Taking into account the metrics presented to evaluate the segmentation results on ocular region components, the one that best quantifies how well a RoI is segmented is the Intersection over Union (IoU) metric. The use of IoU as a

evaluation metric is based on the fact that using this it is possible to compare how close the segmented masks are to the ground-truth.

2.2 Region of Interest Extraction Using Contextual Relationship

In addition to the commonly employed approaches to extract the ocular region components presented in the previous sections, there is a set of techniques that aims to detect/segment elements in an image based on the contextual information in which it is located. The contextual information can be defined as any information that is not directly produced by the appearance of an object, such as, nearby data, image tags, annotations or the presence of other objects [55, 56, 57].

A traditional object categorization approach is made using visual attributes such as color, edges responses, texture, and shapes cues. However, according to Biederman [39], using only these feature sets, understanding a scene composition is not possible. To detect an object based on context, it is necessary to understand the five different classes of relationships between an object and its surroundings: *interposition*, *support*, *probability*, *position*, and *size*. *Interposition* and *support* refer to the physical space. *Probability*, *position*, and *size* are defined as semantic relations once they require access to the referential meaning of the object. Semantic relations include information about specific interactions among objects in the scene, and they are often used as *contextual features*.

Many authors have explored the semantic relationships proposed in [39] aiming to improve the results on recognition task of objects [58, 59, 60, 61, 62, 63]. These relationships can be grouped into three categories: semantic context (*probability*), spatial context (*position*), and scale context (*size*).

Semantic context corresponds to the likelihood of an object to be found in some scenes but not in others. Hence, it is defined in terms of the co-occurrence of one object with others and its occurrence in scenes.

Torralba [58] presented one of the first methods using statistical approaches to detect objects. The proposed technique explores and generalizes the semantic context in a real world scenario, by using the correlation among the statistics of low-level features across the entire scene and the objects it contains. However, the authors do not report either the obtained results or the database employed in this work.

In the same direction of the work proposed by Torralba [58], other authors have employed statistical methods to detect objects based on semantic context [64, 62, 65, 63].

Wolf and Bileschi [64] proposed an approach to extract the semantic context using context features and the Support Vector Machines (SVM) classifier. The presented approach achieved an accuracy of 83.00% (estimated value obtained from a Receiver Operating Characteristics (ROC) curve on that work) on their database named StreetScene. To obtain the context features, the authors proposed a two-stage process. In the first stage, the image is processed to calculate the low level and semantic information. In the second stage, the context feature is calculated at each point by collecting samples of the previously computed features at predefined relative positions.

Rabinovich et al. [62] employed the Conditional Random Field (CRF) to detect the objects in a scene maximizing the labels agreement according to the contextual relevance. Firstly, a fully connected graph among the segmented labels was used. And then, the CRF was trained in more straightforward problems defined on a relatively small number of segments. The proposed approach showed to be competitive with the state-of-the-art achieving 74.20% and 68.40% accuracies on the Pascal VOC 2007 [66] and Microsoft Research Cambridge (MSRC) [67] databases, respectively.

Verbeek and Triggs [65] proposed a segmentation approach that achieves 84.90%, 87.40% and 74.60% of accuracy on the MSRC, Sowerby [61] and Corel¹ databases respectively. These results were obtained using CRF together with unlabeled nodes. This way the unknown labels are marginalized and the log-likelihood of the known labels can be maximized by gradient descent.

Galleguillos et al. [63] introduced a new approach to object categorization based on two types of context (co-occurrence and relative location) using local appearance features, and achieved 36.70% and 68.47% of accuracy, on the Pascal Voc 2007 and MSRC databases respectively. The presented method used CRFs to maximize object label attribution to both semantic and spatial features. The results of that work showed that combining co-occurrence and spatial context improves the accuracy of the system when compared to the results where only co-occurrence data are used in training.

Since the semantic context has been well explored in the literature, Kumar and Hebert [55] proposed a new segmentation approach that explored the spatial context in the images. The proposed approach explore the pairwise relationship in images using a two-layer hierarchical formulation to exploit different levels of contextual information in images. In the first layer, the system it encodes the region's interaction, and in the second, the object's interactions are mapped, as shown in Figure 5. The experiments were performed on four databases: Beach Database [68], Sowerby Database [61],

¹<https://sites.google.com/site/dctresearch/Home/content-based-image-retrieval>

Building/Road/Car dataset [69] and Monitor/Keyboard/Mouse Dataset [69], and the respective accuracies for these are 74.00%, 89.30%, 84.36% and 90.00% respectively (result obtained analyzing a Receiver Operating Characteristics (ROC) curve).

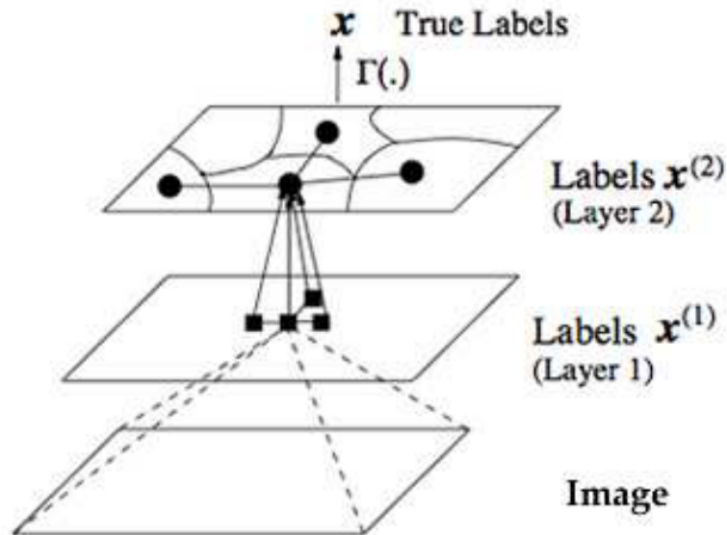


Figura 5: Sample of the architecture proposed by [55].

As we can see, the semantic context is implicitly present in the spatial context, since the information of object co-occurrences come from identifying objects from the spatial relations in the scene. The same happens to scale context, once a contextual relationship establishes that objects have a limited set of size relationships with other objects in the scene. Therefore, the use of spatial and scale context involves using all forms of contextual information in the scene.

Over the years, many approaches have been proposed to extract a region of interest RoI using contextual information. But, only after 2018 the first works that integrate the Biederman’s [39] contextual classes with CNNs were proposed. Leng et al. [70] introduced the Context Learning Network (CLN), which aims to capture the pairwise relationships between objects and the global context of each one. By using the proposed method, the authors achieved 82.10%, 80.70%, and 38.40% of mean Average Precision (mAP) on the Pascal VOC 2007, Pascal VOC 2012, and Coco databases, respectively. The CLN is composed of two subnetworks, a Multi-Layer Perceptron (MLP) which captures the pairwise relationships and a CNN that learns the global context of the image.

Leng et al. [71] also proposed a context-aware U-Net, which focuses on capturing valuable contexts and improving the segmentation performance on the ISBI Challenge Database. For such goal, a lightweight context transfer module was developed to learn the rich context features present in the image. The results obtained are similar to those presented by the state-of-the-art on the ISBI Challenge. To evaluate the results, the authors proposed three metrics: Warping Error, Rand Error, and Pixel Error, their respective achieved values are $1.212e^{-4}\%$, $2.12e^{-2}\%$, and $3.4600e^{-2}\%$.

2.3 Final Remarks

Since, to the best of our knowledge, the specific works present in the literature for the ocular region components detection do not address the use of contextual information, and the works that made use of this approach in the scene understanding scenario present promising results, it is opportune to develop a specific approach for the extraction of the RoI in the ocular region taking into account the contextual information.

3 Methodology

This section presents the proposed architecture addressing the ocular region components (iris and sclera) segmentation, taking into account the contextual information of the region.

To solve the aforementioned segmentation problem, we propose the Ocular Region Context Network (ORCNet), a new architecture that combines the Context Encoding Network (EncNet) presented in [40] with the main contribution of this

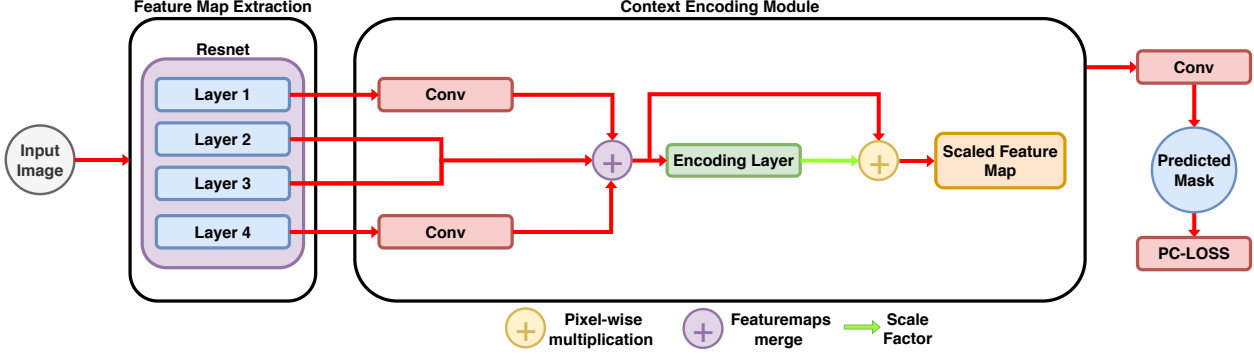


Figure 6: General overview of the proposed approach.

work: the Punish Context Loss (PC-Loss). PC-Loss was inspired in the Biederman’s semantic relationship concepts in which the relationships of objects in an image are evaluated using semantic, scale and spatial context.

In the EncNet, the extraction of feature maps is performed by using a ResNet based backbone, which was chosen because it does not suffer the effects of the vanishing gradient, thus it does not compromise the network overall performance. Once the feature maps are extracted using the ResNet backbone, they were used to feed the *Context Encoding Module*.

The *Context Encoding Module* is composed of an *Encoding Layer* [72] which captures the encoded semantics, a fully connected layer, and a sigmoid as the activation function, which output scaling factors $\gamma = \delta(W_e)$, where W denotes the layer weights and δ is the sigmoid function. Then, the module output is given by $Y = X \otimes \gamma$, where \otimes denotes a channel-wise multiplication between the input feature maps X and scaling factors γ . The channel-wise multiplication is employed to emphasize or de-emphasize class-dependent feature maps.

Once the feature maps are processed by the EncNet, we employ the Punish Context Loss (PC-Loss). The PC-Loss consists of punishing the segmentation *Loss* of the network by using a percentage value obtained, taking into account the Biederman’s[39] relationships, i.e.,

$$\text{PC-Loss} = \frac{\lambda + \rho}{2}, \quad (1)$$

where the parameter λ is the *Scale Context Coefficient* (a value that estimates the average difference in terms of *Jaccard Distance* from a class to all other classes on the addressed problem) of an image and it is defined as:

$$\lambda = \frac{1}{N} \sum_{i=1}^N \frac{1}{N-1} \sum_{\substack{j=1 \\ j \neq i}}^N \sqrt{(\theta_i - \theta_j)^2}, \quad (2)$$

where N is the number of classes present in the evaluated problem, and the θ term is the *Jaccard Distance* obtained by subtracting the *Jaccard similarity coefficient* $J = \frac{gt_i \cap prd_i}{gt_i \cup prd_i}$ from 1, where gt_i and prd_i stand for the ground truth and predicted masks, respectively, i.e.,

$$\theta_i = 1 - J. \quad (3)$$

The ρ parameter is the ratio between the *Spatial Context Coefficient* δ from the ground truth and the predicted segmentation,

$$\rho = \frac{\delta(prd)}{\delta(gt)}. \quad (4)$$

where

$$\delta = \frac{1}{N} \sum_{i=1}^N \frac{1}{N-1} \sum_{\substack{j=1 \\ i \neq j}}^N \sqrt{(C_i - C_j)^2}, \quad (5)$$

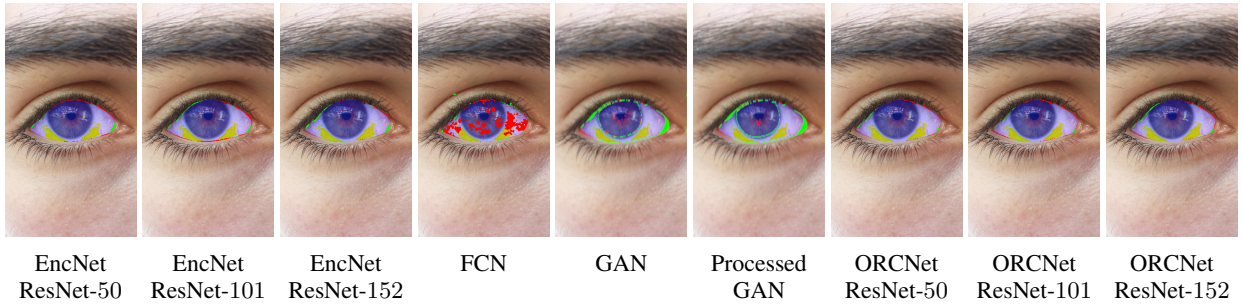
C the center of mass from an evaluated object. Considering that an object consists of n distinct points $x_1 \dots x_n$, then the centroid (center of mass) is given by,

$$C = \frac{1}{n} \sum_{i=1}^n x_i. \quad (6)$$

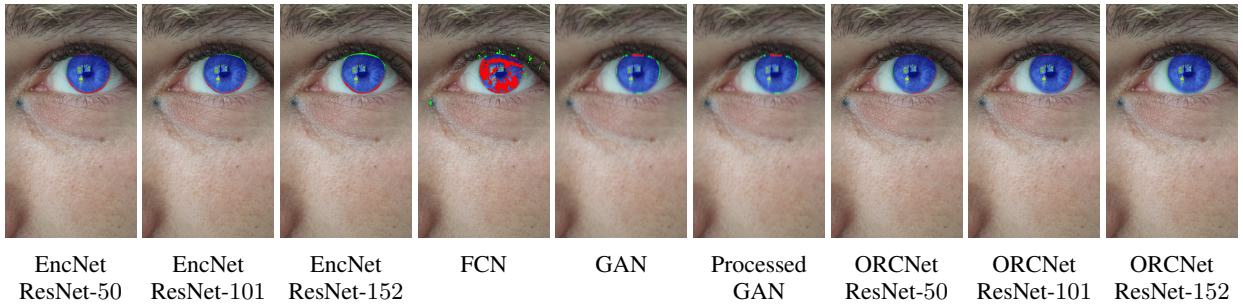
The ORCNet implementation was made in the PyTorch framework, and to perform the training we adopted a learning rate of 10^{-4} combined with a momentum of 0.9 during 1000 epochs.

4 Experiments

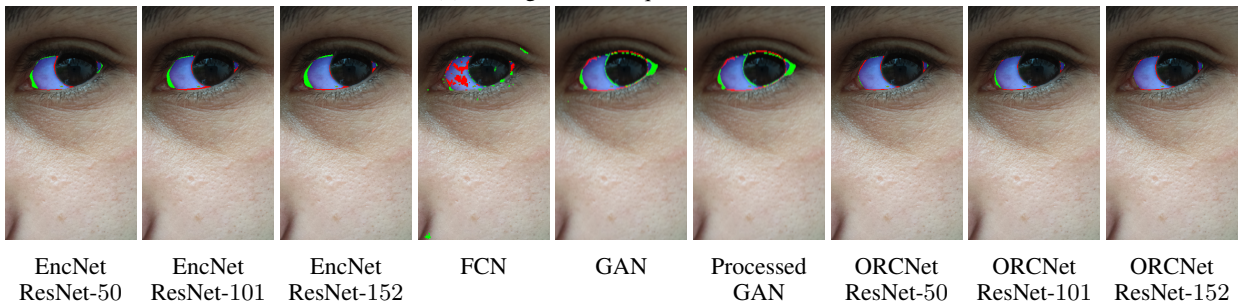
In this section, we present the database, the evaluation protocol and the state-of-the-art segmentation approaches employed as baselines used in this work. The experiments were carried out on the MICHE-I database, which is described in Section 4.1. Note that we evaluate the networks on each MICHE-I subset separately. All experiments were performed on a computer with an AMD[®] Ryzen[™] 7 2700X 4.40GHz CPU, 32 GB of RAM and two NVIDIA Titan V GPUs.



(a) All scenario segmentation qualitative results



(b) Iris segmentation qualitative results



(c) Sclera segmentation qualitative results

Figure 7: Qualitative results achieved by the ORCNet, and by the proposed baselines. Green and red pixels represent False Positive (FP) and FP, respectively.

4.1 Databases

To evaluate the performance of our proposed approach to solve the problem of iris and sclera simultaneous segmentation, the MICHE-I database was employed. The database was chosen because it is composed of 3, 191 non-processed images captured using three different devices (see Table 1). The devices used to capture the images of the database are:

- Samsung Galaxy S4 (GS4) smartphone: Google Android operating system, two sensors: a Complementary Metal-Oxide-Semiconductor (CMOS) sensor with 13 Megapixel (72 dpi) and 2322×4128 resolution, and a CMOS sensor with 2 Megapixel (72) and 1080×1920 resolution;
- Samsung Galaxy Tab 2 tablet: Google Android Operating System, one sensor with 0.3 megapixel (72 dpi) and 640×480 resolution;
- Apple iPhone 5 smartphone: Apple iOS Operating System, two sensors: a CMOS sensor with 8 Megapixel (72 dpi) and 1536×2048 resolution, and a CMOS sensor with 1.2 Megapixel (72 dpi) and 960×1280 resolution.

Tabela 1: Overview of the databases used in this work [73].

Database	Images	Subjects	Resolution
MICHE-GS4	1,297	92	2322×4128 and 1080×1920
MICHE-GT2	632	92	640×480
MICHE-IP5	1,262	92	1536×2048 and 960×1280

The non-processed images are the ones that, in addition to the components of the ocular region, the images also have parts of the face and even other types of objects (background objects, glasses, nose, mouth) as can be seen in Fig. 8, which makes the segmentation task even more challenging.

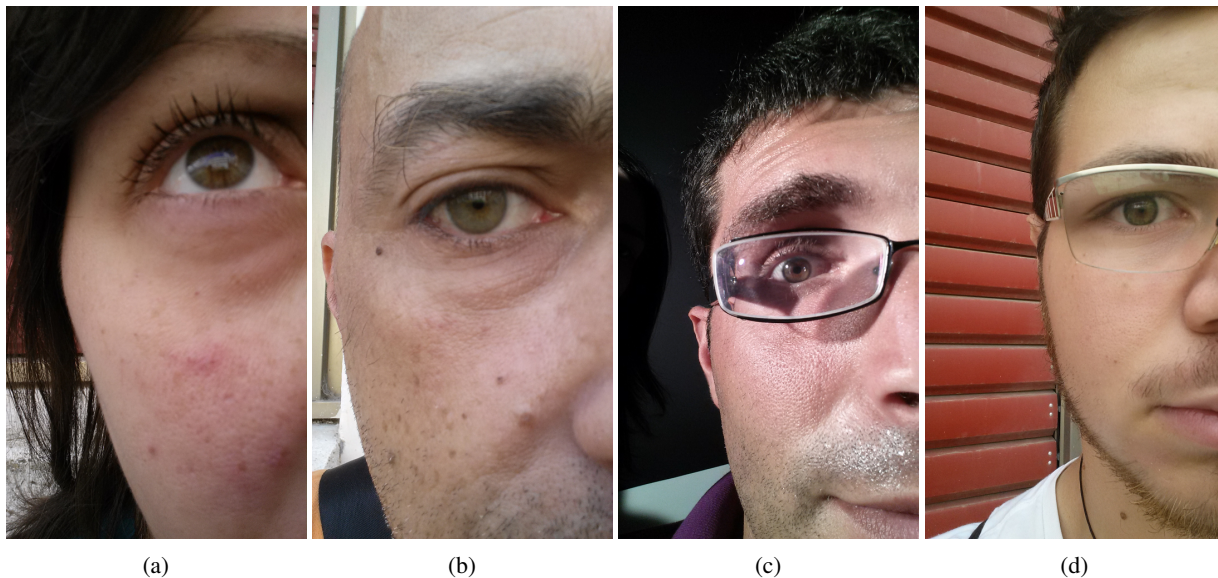


Figura 8: Samples of difficult images

4.2 Evaluation Protocol

The evaluation of an automatic detection approach is performed in a pixel-to-pixel comparison between the ground truth and the predicted segmentation mask. Therefore, we use the mean F -score, Intersection over Union (IoU) and Error Rate (ER) evaluation metrics.

In order to perform a fair evaluation and comparison of the proposed approaches, we divided each database into three subsets, being 40% of the images for training, 40% for testing and 20% for validation. We adopted this protocol (i.e., with a larger test set) to provide more samples for the sake of statistical significance. In addition, we perform the Wilcoxon signed-rank test [74] with significance level of $\alpha = 0.05$ to verify if there is a statistical difference between the detection approaches.

4.3 Baselines

We selected three baseline frameworks described (and available) in the literature to compare to our approach: Enc-Net [40], Fully Convolutional Network (FCN) [54] and Generative Adversarial Network (GAN) [53].

The FCN and the GAN segmentation approaches were chosen as baseline methods because they presented promising results on sclera and iris segmentation tasks [25, 26]. The EncNet approach was chosen since the *Context Encoding Module* proposed in it encodes the contextual information in the image, thus outperforming the conventional segmentation approaches employed in many different research areas.

The FCN segmentation approach was proposed in [54]. The network has only convolutional layers and the segmentation process can take input images of arbitrary sizes, producing correspondingly-sized output with efficient inference and learning.

In this work, we employ the FCN approach presented by Teichmann et al. [75]. As shown in Figure 9, features are extracted using a CNN without the fully connected layers (i.e., VGG-16 without the last 3 layers).

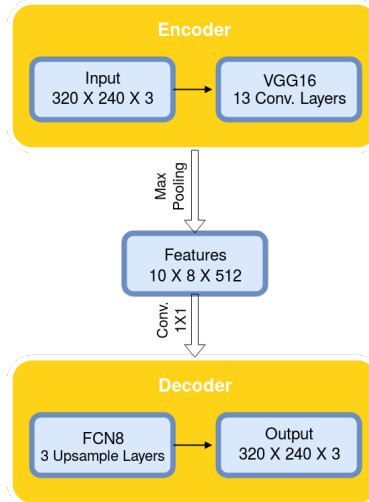


Figura 9: FCN architecture employed in the simultaneous ocular region components segmentation.

Next, the extracted features pass through two 1×1 convolutional layers, generating an output of dimension $10 \times 8 \times 6$. The output of these convolutional layers is processed by the FCN8 architecture proposed in [54], which performs the up sampling combining the last three layers from the VGG-16.

GANs are a type of deep neural network composed of a generator and a discriminator networks, which pits one against the other. In a first moment the generator network receives noise as input and generates sample images, and the discriminator network evaluates how close the ground truth is to the generated images [53]. A generic GAN architecture is shown in Fig. 10.

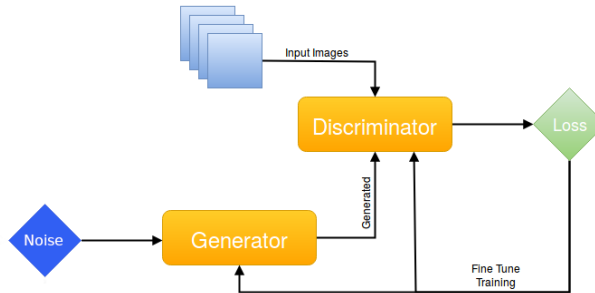


Figura 10: GAN architecture employed in the simultaneous ocular region components segmentation.

Basically, the generator network learns to produce more realistic samples throughout each iteration, and the discriminator network learns to better distinguish between real and synthetic data.

The GAN approach [76] used in this work, which is a conditional GAN able to learn the relation between an image and its label file. This network is able to generate a variety of image types, which can be employed in various tasks such as photo generation and semantic segmentation. Since the results obtained by the GAN approach presented some small noise particles, we employed, as a post processing stage, mathematical morphology to remove them, and the results obtained by this method are presented in the Section 4.

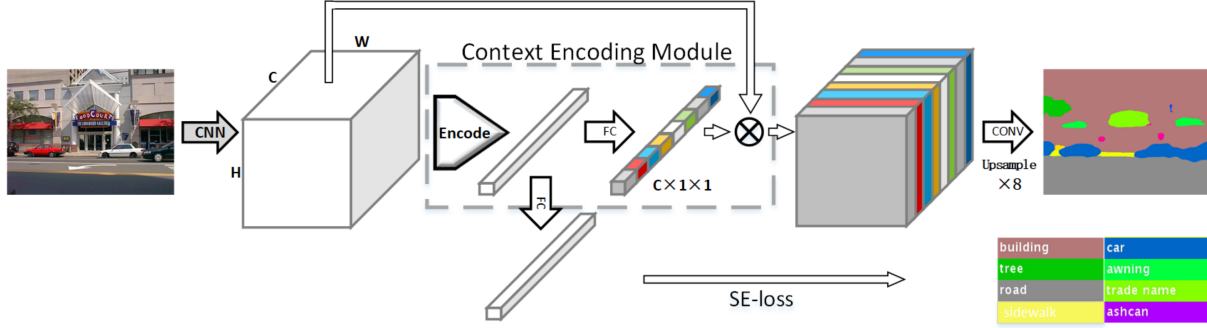


Figura 11: EncNet architecture [40] employed in the simultaneous ocular region components segmentation.

The **EncNet** presented in [40] captures the global information of an image to improve scene segmentation. The model uses the ResNet as feature extractor and uses the extracted features to feed a Context Encoding Module inspired by the Encoding Layer presented in [72].

The Context Encoding Module learns visual centers and smoothing factors to create an embedding taking into account the contextual information while highlighting class-dependent feature maps. The module is composed of scaling factors to learn the contextual information using fully connected layers, and by a Semantic Encoding Loss (SE-Loss) to regularize the training of the module by detecting the presence of object classes. The outputs of the Context Encoding Module are reshaped and processed by a dilated convolution strategy while minimizing the SE-Losses and the final pixel-wise loss, as illustrated in Figure 11.

Tabela 2: Wilcoxon signed-rank results taking into account the sclera segmentation scenario in the MICHE-I dataset.

	RoI	EncNet ResNet 50	EncNet ResNet 101	EncNet ResNet 152	FCN	GAN	GAN PROCESSED	OrcNet ResNet 50	OrcNet ResNet 101	OrcNet ResNet 152
midrule	EncNet ResNet-50	-	1.33 ⁻³	1.02 ⁻⁵	8.38 ⁻⁸⁰	8.56 ⁻⁷⁵	7.22 ⁻⁶⁶	7.22 ⁻⁷²	2.61 ⁻⁷⁰	3.85 ⁻⁶⁷
	EncNet ResNet-101	1.33 ⁻³	-	3.03 ⁻¹⁰	3.29 ⁻⁷⁵	6.10 ⁻⁶⁴	4.34 ⁻⁵⁶	1.19 ⁻⁷¹	2.79 ⁻⁷⁶	4.61 ⁻⁷³
	EncNet ResNet-152	1.02 ⁻⁵	3.03 ⁻¹⁰	-	1.56 ⁻⁸⁰	1.00 ⁻⁷⁴	4.22 ⁻⁶⁹	2.24 ⁻⁶³	1.05 ⁻⁶⁴	3.13 ⁻⁶⁴
	FCN	8.38 ⁻⁸⁰	3.29 ⁻⁷⁵	1.56 ⁻⁸⁰	-	1.75 ⁻⁵³	9.50 ⁻⁶⁷	4.07 ⁻⁸²	9.58 ⁻⁸⁴	2.01 ⁻⁸¹
	GAN	8.56 ⁻⁷⁵	6.10 ⁻⁶⁴	1.00 ⁻⁷⁴	1.75 ⁻⁵³	-	9.78 ⁻⁷⁶	5.15 ⁻⁷⁶	4.26 ⁻⁷⁶	4.38 ⁻⁸⁰
	GAN PROCESSED	7.22 ⁻⁶⁶	4.34 ⁻⁵⁶	4.22 ⁻⁶⁹	9.50 ⁻⁶⁷	9.78 ⁻⁷⁶	-	7.91 ⁻⁷⁵	6.76 ⁻⁷⁵	1.19 ⁻⁷⁷
	OrcNet ResNet-50	7.22 ⁻⁷²	1.19 ⁻⁷¹	2.24 ⁻⁶³	4.07 ⁻⁸²	5.15 ⁻⁷⁶	7.91 ⁻⁷⁵	-	9.69 ⁻³	1.78 ⁻⁰²
	OrcNet ResNet-101	2.61 ⁻⁷⁰	2.79 ⁻⁷⁶	1.05 ⁻⁶⁴	9.58 ⁻⁸⁴	4.26 ⁻⁷⁶	6.76 ⁻⁷⁵	9.69 ⁻³	-	1.29 ⁻⁰⁴
	OrcNet ResNet-152	3.85 ⁻⁶⁷	4.61 ⁻⁷³	3.13 ⁻⁶⁴	2.01 ⁻⁸¹	4.38 ⁻⁸⁰	1.19 ⁻⁷⁷	1.78 ⁻⁰²	1.29 ⁻⁰⁴	-
Iris	EncNet ResNet-50	-	8.36 ⁻³	8.97 ⁻³	1.58 ⁻⁸¹	8.25 ⁻⁴⁴	6.06 ⁻⁴⁷	8.63 ⁻⁴⁸	3.14 ⁻⁴⁵	9.97 ⁻⁴⁷
	EncNet ResNet-101	8.36 ⁻³	-	6.03 ⁻³	3.48 ⁻⁷⁶	3.42 ⁻³⁶	1.66 ⁻³⁸	6.86 ⁻³⁵	4.71 ⁻⁴⁶	1.30 ⁻⁴³
	EncNet ResNet-152	8.97 ⁻³	6.03 ⁻³	-	9.50 ⁻⁸³	1.17 ⁻⁴³	1.04 ⁻⁴⁶	1.90 ⁻³⁹	4.60 ⁻⁴⁷	3.24 ⁻⁴⁸
	FCN	1.58 ⁻⁸¹	3.48 ⁻⁷⁶	9.50 ⁻⁸³	-	2.42 ⁻⁷⁵	1.28 ⁻⁷²	1.86 ⁻⁷⁹	1.14 ⁻⁸⁰	2.85 ⁻⁷⁹
	GAN	8.25 ⁻⁴⁴	3.42 ⁻³⁶	1.17 ⁻⁴³	2.42 ⁻⁷⁵	-	1.87 ⁻²⁴	1.34 ⁻⁶⁵	9.61 ⁻⁶⁷	1.02 ⁻⁶⁹
	GAN PROCESSED	6.06 ⁻⁴⁷	1.66 ⁻³⁸	1.04 ⁻⁴⁶	1.04 ⁻⁴⁶	1.87 ⁻²⁴	-	1.56 ⁻⁶⁶	1.68 ⁻⁶⁷	1.94 ⁻⁷⁰
	OrcNet ResNet-50	8.63 ⁻⁴⁸	6.86 ⁻³⁵	1.90 ⁻³⁹	1.86 ⁻⁷⁹	1.34 ⁻⁶⁵	1.56 ⁻⁶⁶	-	2.77 ⁻¹	3.75 ⁻³
	OrcNet ResNet-101	3.14 ⁻⁴⁵	4.71 ⁻⁴⁶	4.60 ⁻⁴⁷	1.14 ⁻⁸⁰	9.61 ⁻⁶⁷	1.68 ⁻⁶⁷	2.77 ⁻¹	-	3.49 ⁻⁴
	OrcNet ResNet-152	9.97 ⁻⁴⁷	1.30 ⁻⁴³	3.24 ⁻⁴⁸	2.85 ⁻⁷⁹	1.02 ⁻⁶⁹	1.94 ⁻⁷⁰	3.75 ⁻³	3.49 ⁻⁴	-
Sclera	EncNet ResNet-50	-	9.22 ⁻⁰³	8.23 ⁻⁴	3.12 ⁻⁷⁷	2.75 ⁻⁴⁰	1.62 ⁻³²	2.93 ⁻⁶⁸	6.67 ⁻⁶⁶	2.60 ⁻⁷²
	EncNet ResNet-101	9.22 ⁻³	-	1.99 ⁻⁵	5.77 ⁻⁷⁵	2.18 ⁻³¹	9.22 ⁻²⁴	6.12 ⁻⁶⁷	1.41 ⁻⁷²	4.23 ⁻⁷⁷
	EncNet ResNet-152	8.23 ⁻⁴	1.99 ⁻⁵	-	2.94 ⁻⁷⁷	1.67 ⁻⁴¹	6.73 ⁻³³	1.00 ⁻⁶⁴	1.47 ⁻⁶⁸	4.99 ⁻⁷⁶
	FCN	3.12 ⁻⁷⁷	5.77 ⁻⁷⁵	2.94 ⁻⁷⁷	-	1.30 ⁻⁶⁷	2.81 ⁻⁷¹	6.62 ⁻⁸³	7.03 ⁻⁸³	4.21 ⁻⁸³
	GAN	2.75 ⁻⁴⁰	2.18 ⁻³¹	1.67 ⁻⁴¹	1.30 ⁻⁶⁷	-	1.74 ⁻²⁶	1.23 ⁻⁷⁴	1.35 ⁻⁷⁵	2.33 ⁻⁷⁸
	GAN PROCESSED	1.62 ⁻³²	9.22 ⁻²⁴	6.73 ⁻³³	2.81 ⁻⁷¹	1.74 ⁻²⁶	-	2.06 ⁻⁷²	6.32 ⁻⁷³	3.76 ⁻⁷⁶
	OrcNet ResNet-50	2.93 ⁻⁶⁸	6.12 ⁻⁶⁷	1.00 ⁻⁶⁴	6.62 ⁻⁸³	1.23 ⁻⁷⁴	2.06 ⁻⁷²	-	4.85 ⁻³	1.29 ⁻¹³
	OrcNet ResNet-101	6.67 ⁻⁶⁶	1.41 ⁻⁷²	1.47 ⁻⁶⁸	7.03 ⁻⁸³	1.35 ⁻⁷⁵	6.32 ⁻⁷³	4.85 ⁻³	-	9.48 ⁻¹³
	OrcNet ResNet-152	2.60 ⁻⁷²	4.23 ⁻⁷⁷	4.99 ⁻⁷⁶	4.21 ⁻⁸³	2.33 ⁻⁷⁸	3.76 ⁻⁷⁶	1.29 ⁻¹³	9.48 ⁻¹³	-

5 Results and Discussion

The experiments were carried out using the protocol presented in Section 4.2. To validate, evaluate and compare the proposed approaches, we report the F - Score, the Intersection over Union (IoU), and Error Rate (ER), respectively.

Table 3 presents the mean results obtained in the performed experiments. This table is divided into three sections, one to each segmentation scenario (ALL (Iris and Sclera are considered as a unique region), Iris and Sclera). For each one of the scenarios, four segmentation approaches were evaluated, that is, EncNet, FCN, GAN, and our proposal ORCNet. Table 4 in turn presents the individual result for each MICHE-I database subset for the same scenario division presented in Table 3.

Yet, regarding the employed segmentation approaches, it is necessary to highlight that for the EncNet, ORCNet, and GAN approaches, more than one segmentation approach was employed. For the EncNet and ORCNet three segmentation variants were proposed, being the ResNet backbone (ResNet-50, ResNet-101 and ResNet-152) the difference among them. For the GAN approach, two different approaches were employed, one based on the method proposed by [53] and another one in which small noise particles in the output images were removed by mathematical morphology operations.

By analyzing the obtained results presented in Table 3, we observed that in all of the segmentation scenarios —ALL(Iris + Sclera), Iris and Sclera—, the ORCNet approach presented the best results in terms of $F - Score$, Intersection over Union (IoU), and Error Rate (ER). Also, it is important to observe that independently from the used ResNet backbone, the proposed ORCNet approach outperforms all the baselines evaluated in this work. Finally, we verify if there was a statistical difference on the obtained results. Employing the Wilcoxon signed-rank, we conclude that there is statistical difference between the proposed architecture and the state-of-the-art approaches used as baseline as shown in Table 2.

Once a general analysis of the performance obtained with the ORCNet was presented, we can individually discuss the results obtained in each of the scenarios evaluated using the protocol proposed in Section 4.2. In ALL segmentation scenario, we observed that the mean $F - Score$ obtained by using the ORCNet ResNet-152 is 95.67%, outperforming the best baseline (EncNet ResNet-152) score by 1.42%. In terms of ER the obtained score outperforms the best baseline by 33%, reducing the error rate of 0.39% to 0.26%. Finally, by analyzing the IoU, we observed that in the ALL segmentation scenario, the proposed approach achieved a score of 90.97%, outperforming the best baseline result by 5.04%.

The behaviour presented in the ALL (iris + sclera) segmentation scenario can also be seen in the iris and sclera individual segmentation tasks, since the best results were obtained by using the ORCNet. In the Iris segmentation the mean F-Score, ER and IoU obtained values are 95.91%, 0.15% and 91.17% outperforming the best baseline results by 0.89%, 25% and 3.22% respectively. And, in the sclera segmentation the mean F-Score, ER and IoU obtained values are 89.78%, 0.24% and 80.90%, outperforming the best results by 4.50%, 26.47% and 11.01%, respectively.

In addition to presenting better results in relation to the baselines, we also found that the standard deviation presented by the results was smaller when the context based segmentation was employed. In this way it is possible to state that the ORCNet presented most stable segmentation of the Region of Interest (RoI), since it showed less variability in the segmentation masks. Finally, it is important to highlight that regardless of the backbone used as feature maps extractor in ORCNet, the proposed approach outperforms all the baselines evaluated.

5.1 Visual Analysis

Here, we perform a visual analysis of some segmented images by the baselines and the proposed architecture. Fig. 7 shows segmentation samples of the three evaluated scenarios (*ALL*, *iris* and *sclera*) performed by the ORCNet approach, as well as the state-of-the-art segmentation approaches employed as baselines.

By analyzing the segmentation results presented in Fig. 7, it is possible to observe that the results obtained using the ORCNet approach was slightly better if compared with the baseline approaches. In all the evaluated segmentation scenarios (ALL(Iris + Sclera), iris and sclera), the proposed approach with a ResNet-152 backbone, performed a better segmentation since fewer pixels were wrongly segmented (green area) while the number of pixels that have not been targeted is also less than that presented by other approaches (red area).

6 Conclusion

This work introduced the Ocular Region Context Network (ORCNet), a new approach that uses the Punish Context Loss (PC-Loss) to simultaneously segment the ocular region components using the contextual information. PC-Loss was implemented, evaluated and compared with baseline methods (EncNet, FCN and GAN). The proposed approach attained better Intersection over Union (IoU), Error Rate (ER) and $F - Score$ values in all the evaluated scenarios (*general*, *iris* and *sclera* segmentations).

Taking into account the presented results it is necessary to emphasize that the only difference between the EncNet and the ORCNet segmentation approaches is the use of the PC-Loss. By using the PC-Loss, we observe that the use of contextual information improve the results of a simultaneous iris and sclera segmentation independent of the architecture used. Once it was found that the use of contextual information improve the segmentation results, we prove the hypothesis of this work and answer the main question with “it is possible to improve the ocular region components extraction by analyzing the context present in the images”.

Tabela 3: Performance comparison among the baseline approaches and the proposed ORCNet approach employing the MICHE-I dataset as input data. Intersection over Union (IoU) is considered as the prior measure ranking methods.

Approach	RoI	F-Score	ER	IoU
EncNet ResNet-50	ALL	94.21 ± 4.97	0.39 ± 0.29	86.51 ± 13.31
EncNet ResNet-101		94.23 ± 5.29	0.39 ± 0.29	85.90 ± 14.51
EncNet ResNet-152		94.33 ± 5.54	0.39 ± 0.31	86.60 ± 13.92
FCN		83.53 ± 11.06	1.08 ± 1.12	72.79 ± 14.97
GAN		89.80 ± 8.56	0.67 ± 0.42	82.10 ± 11.67
GAN PROCESSED		91.04 ± 9.22	0.57 ± 0.41	84.25 ± 11.90
ORCNet ResNet-50		95.41 ± 4.22	0.27 ± 0.21	90.30 ± 10.56
ORCNet ResNet-101		95.51 ± 4.30	0.27 ± 0.21	90.64 ± 9.92
ORCNet ResNet-152		95.67 ± 4.01	0.26 ± 0.22	90.97 ± 9.35
EncNet ResNet-50		Iris	94.91 ± 5.63	0.20 ± 0.19
EncNet ResNet-101	94.99 ± 5.69		0.20 ± 0.19	87.92 ± 15.43
EncNet ResNet-152	95.06 ± 5.39		0.20 ± 0.20	88.32 ± 14.70
FCN	80.73 ± 12.19		0.63 ± 0.62	68.58 ± 16.43
GAN	88.35 ± 9.89		0.38 ± 0.31	79.48 ± 14.77
GAN PROCESSED	89.14 ± 9.54		0.36 ± 0.30	80.26 ± 15.36
ORCNet ResNet-50	95.62 ± 4.81		0.16 ± 0.18	90.42 ± 12.56
ORCNet ResNet-101	95.70 ± 5.46		0.16 ± 0.18	90.82 ± 11.97
ORCNet ResNet-152	95.91 ± 4.96		0.15 ± 0.16	91.17 ± 11.75
EncNet ResNet-50	Sclera		85.74 ± 10.15	0.34 ± 0.24
EncNet ResNet-101		85.60 ± 9.79	0.34 ± 0.23	72.48 ± 17.89
EncNet ResNet-152		85.91 ± 10.25	0.34 ± 0.26	72.87 ± 17.93
FCN		72.41 ± 15.49	0.74 ± 0.67	57.35 ± 17.33
GAN		90.35 ± 13.17	0.58 ± 0.36	68.34 ± 15.21
GAN PROCESSED		82.02 ± 12.19	0.51 ± 0.33	70.26 ± 14.94
ORCNet ResNet-50		89.42 ± 7.54	0.25 ± 0.19	80.14 ± 13.61
ORCNet ResNet-101		89.46 ± 7.61	0.25 ± 0.20	80.40 ± 13.11
ORCNet ResNet-152		89.78 ± 6.97	0.25 ± 0.20	80.90 ± 12.84

Additionally, we also manually labeled 3,191 images from the MICHE-I dataset for sclera and iris segmentation. These masks were made available to the research community, enabling other researchers to fairly compare their proposals on the same tasks and also among published works.

There is still room for improvements in the simultaneous segmentation of iris and ocular region research field. As future work, we intend to: (i) design new and better network architectures; (ii) design a general and independent sensor approach, where the image sensor is firstly classified and then the iris and the ocular region are simultaneously segmented with a specific approach trained for a particular image sensor; (iii) compare the proposed context based segmentation approach with methods applied in other domains; (iv) design a new multi-task approach for simultaneously detecting and segmenting the components of the ocular region, taking into account the contextual information of the images.

Referências

- [1] Ruud M. Bolle, Jonathan H. Connell, Sharath Pankanti, Nalini K. Ratha, and Andrew W. Senior. *Guide to Biometrics*. Springer Publishing Company, Incorporated, 2004.
- [2] Kevin W. Bowyer, Karen Hollingsworth, and Patrick J. Flynn. Image understanding for iris biometrics: A survey. *Computer Vision and Image Understanding*, 110(2):281–307, 2008.
- [3] A. Das, U. Pal, M. A. F. Ballester, and M. Blumenstein. Sclera recognition using dense-SIFT. In *13th Int. Conf. on Intelligent Systems Design and Applications*, pages 74–79, Dec 2013.
- [4] Z. Zhou, E. Y. Du, N. L. Thomas, and E. J. Delp. A new human identification method: Sclera recognition. *IEEE Transactions on Systems, Man, and Cybernetics - Part A: Systems and Humans*, 42(3):571–583, May 2012.
- [5] Anil K. Jain, Karthik Nandakumar, and Arun Ross. 50 years of biometric research: Accomplishments, challenges, and opportunities. *Pattern Recognition Letters*, 79:80–105, 2016.
- [6] R. P. Wildes. Iris recognition: an emerging biometric technology. *Proceedings of the IEEE*, 85(9):1348–1363, Sep 1997.

- [7] Luiz A Zanlorensi, Eduardo Luz, Rayson Laroca, Alceu S Britto, Luiz S Oliveira, and David Menotti. The impact of preprocessing on deep representations for iris recognition on unconstrained environments. In *2018 31st SIBGRAPI Conference on Graphics, Patterns and Images (SIBGRAPI)*, pages 289–296. IEEE, 2018.
- [8] Nianfeng Liu, Man Zhang, Haiqing Li, Zhenan Sun, and Tieniu Tan. Deepiris: Learning pairwise filter bank for heterogeneous iris verification. *Pattern Recognition Letters*, 82:154 – 161, 2016. An insight on eye biometrics.
- [9] L. A. Zanlorensi, R. Laroca, E. Luz, A. S. Britto Jr., L. S. Oliveira, and D. Menotti. Ocular recognition databases and competitions: A survey. *arXiv preprint*, arXiv:1911.09646:1–20, 2019.
- [10] G. Mahalingam, K. Ricanek, and A. M. Albert. Investigating the periocular-based face recognition across gender transformation. *IEEE Transactions on Information Forensics and Security*, 9(12):2180–2192, 2014.
- [11] Unsang Park, Raghavender Reddy Jillela, Arun Ross, and Anil K. Jain. Periocular biometrics in the visible spectrum. *IEEE Transactions on Information Forensics and Security*, 6(1):96–106, 2011.
- [12] Chun Wei Tan and Ajay Kumar. Towards online iris and periocular recognition under relaxed imaging constraints. *IEEE Transactions on Image Processing*, 22(10):3751–3765, 2013.
- [13] Chandrashekhhar N. Padole and Hugo Proença. Periocular recognition: Analysis of performance degradation factors. In *2012 5th IAPR International Conference on Biometrics (ICB)*, pages 439–445. IEEE, mar 2012.
- [14] Alaa S. Al-Waisy, Rami Qahwaji, Stanley Ipson, Shumoos Al-Fahdawi, and Tarek A. M. Nagem. A multi-biometric iris recognition system based on a deep learning approach. *Pattern Analysis and Applications*, 21(3):783–802, Aug 2018.
- [15] K. Nguyen, C. Fookes, A. Ross, and S. Sridharan. Iris recognition with off-the-shelf cnn features: A deep learning perspective. *IEEE Access*, 6:18848–18855, 2018.
- [16] H. Proença and J. C. Neves. Irina: Iris recognition (even) in inaccurately segmented data. In *2017 IEEE Conference on Computer Vision and Pattern Recognition (CVPR)*, pages 6747–6756, July 2017.
- [17] Eduardo Luz, Gladston Moreira, Luiz Antonio Zanlorensi Junior, and David Menotti. Deep periocular representation aiming video surveillance. *Pattern Recognition Letters*, 114:2 – 12, 2018. Data Representation and Representation Learning for Video Analysis.
- [18] H. Proença and J. C. Neves. Deep-prwis: Periocular recognition without the iris and sclera using deep learning frameworks. *IEEE Transactions on Information Forensics and Security*, 13(4):888–896, April 2018.
- [19] A. Das, U. Pal, M. A. Ferrer, and M. Blumenstein. SSRBC. In *2016 Int. Conf. on Biometrics (ICB)*, pages 1–6, June 2016.
- [20] A. Das, U. Pal, M. A. Ferrer, M. Blumenstein, D. Štepec, P. Rot, Ž. Emeršič, P. Peer, Š. Struc, S. V. A. Kumar, and B. S. Harish. SSERBC 2017: Sclera segmentation and eye recognition benchmarking competition. In *IEEE International Joint Conference on Biometrics (IJCB)*, pages 742–747, Oct 2017.
- [21] K. V. Delna, K. A. Sneha, and R. P. Aneesh. Sclera vein identification in real time using single board computer. In *2016 Int. Conf. on Next Generation Intelligent Systems (ICNGIS)*, pages 1–5, Sept 2016.
- [22] J. Daugman. New methods in iris recognition. *IEEE TSMC, Part B*, 37(5):1167–1175, 2007.
- [23] Evair Severo, Rayson Laroca, Cides S. Bezerra, Luiz A. Zanlorensi, Daniel Weingaertner, Gladston Moreira, and David Menotti. A benchmark for iris location and a deep learning detector evaluation. In *2018 International Joint Conference on Neural Networks (IJCNN)*, pages 1–7, July 2018.
- [24] D. R. Lucio, R. Laroca, L. A. Zanlorensi, G. Moreira, and D. Menotti. Simultaneous iris and periocular region detection using coarse annotations. In *Conference on Graphics, Patterns and Images (SIBGRAPI)*, pages 178–185, Oct 2019.
- [25] Cides S Bezerra, Rayson Laroca, Diego R Lucio, Evair Severo, Lucas F Oliveira, Alceu S Britto, and David Menotti. Robust iris segmentation based on fully convolutional networks and generative adversarial networks. In *2018 31st SIBGRAPI Conference on Graphics, Patterns and Images (SIBGRAPI)*, pages 281–288. IEEE, 2018.
- [26] D. R. Lucio, R. Laroca, E. Severo, A. S. Britto Jr., and D. Menotti. Fully convolutional networks and generative adversarial networks applied to sclera segmentation. In *IEEE International Conference on Biometrics Theory, Applications and Systems (BTAS)*, pages 1–7, Oct 2018.
- [27] A. K. Jain, A. Ross, and S. Prabhakar. An introduction to biometric recognition. *IEEE Transactions on Circuits and Systems for Video Technology*, 14(1):4–20, Jan 2004.
- [28] A. Rattani and R. Derakhshani. Ocular biometrics in the visible spectrum: A survey. *Image and Vision Computing*, 59:1–16, 2017.

- [29] X. Liu, K. W. Bowyer, and P. J. Flynn. Experiments with an improved iris segmentation algorithm. In *IEEE AutoID'05*, pages 118–123, 2005.
- [30] H. Proença and L. A. Alexandre. Iris segmentation methodology for non-cooperative recognition. *IEE Proceedings - Vision, Image and Signal Processing*, 153(2):199–205, 2006.
- [31] Elhoussaine Ouabida, Abdelaziz Essadique, and Abdenbi Bouzid. Vander lugt correlator based active contours for iris segmentation and tracking. *Expert Systems with Applications*, 71:383–395, 2017.
- [32] S. Shah and A. Ross. Iris segmentation using geodesic active contours. *IEEE Transactions on Information Forensics and Security*, 4(4):824–836, Dec 2009.
- [33] Tieniu Tan, Zhaofeng He, and Zhenan Sun. Efficient and robust segmentation of noisy iris images for non-cooperative iris recognition. *Image and Vision Computing*, 28(2):223–230, feb 2010.
- [34] P. Podder, T. Z. Khan, M. H. Khan, M. M. Rahman, R. Ahmed, and M. S. Rahman. An efficient iris segmentation model based on eyelids and eyelashes detection in iris recognition system. In *Int. Conf. on Computer Communication and Informatics*, pages 1–7, 2015.
- [35] M. Haindl and M. Krupička. Unsupervised detection of non-iris occlusions. *Pattern Recognition Letters*, 57:60–65, 2015.
- [36] E. Jalilian, A. Uhl, and R. Kwitt. Domain adaptation for cnn based iris segmentation. In *Int. Conf. of the Biometrics Special Interest Group (BIOSIG)*, pages 1–6, Sept 2017.
- [37] N. Liu, H. Li, M. Zhang, Jing Liu, Z. Sun, and T. Tan. Accurate iris segmentation in non-cooperative environments using fully convolutional networks. In *Int. Conf. on Biometrics*, pages 1–8, June 2016.
- [38] L. A. Zanlorensi, H. Proença, and D. Menotti. Unconstrained periocular recognition: Using generative deep learning frameworks for attribute normalization. *arXiv preprint*, arXiv:2002.03985:1–5, 2020.
- [39] Irving Biederman. Perceiving real-world scenes. *Science*, 177(4043):77–80, 1972.
- [40] Hang Zhang, Kristin Dana, Jianping Shi, Zhongyue Zhang, Xiaogang Wang, Amrith Tyagi, and Amit Agrawal. Context encoding for semantic segmentation. In *Proceedings of the IEEE Conference on Computer Vision and Pattern Recognition*, pages 7151–7160, 2018.
- [41] D. Osorio-Roig, C. Rathgeb, M. Gomez-Barrero, A. Morales-González, E. Garea-Llano, and C. Busch. Visible wavelength iris segmentation: A multi-class approach using fully convolutional neuronal networks. In *2018 International Conference of the Biometrics Special Interest Group (BIOSIG)*, pages 1–5, 2018.
- [42] Peter Rot, Žiga Emeršič, Vitomir Struc, and Peter Peer. Deep multi-class eye segmentation for ocular biometrics. In *2018 IEEE International Work Conference on Bioinspired Intelligence (IWOB)*, pages 1–8, 2018.
- [43] W. Zhang and Y. Ma. A new approach for iris localization based on an improved level set method. In *2014 11th International Computer Conference on Wavelet Active Media Technology and Information Processing (ICCWAMTIP)*, pages 309–312, Dec 2014.
- [44] CASIA. Casia version 4 database, 2010.
- [45] Julian Fierrez, Javier Ortega-Garcia, Doroteo Torre Toledano, and Joaquin Gonzalez-Rodriguez. Biosec baseline corpus: A multimodal biometric database. *Pattern Recognition*, 40(4):1389–1392, 2007.
- [46] Tejas Indulal Dhamecha, Richa Singh, Mayank Vatsa, and Ajay Kumar. Recognizing disguised faces: Human and machine evaluation. *PloS one*, 9(7), 2014.
- [47] Hugo Proença and Lus A. Alexandre. Toward covert iris biometric recognition: Experimental results from the NICE contests. *IEEE Trans. on Information Forensics and Security*, 7(2):798–808, 2012.
- [48] Ana Sequeira, Lulu Chen, Peter Wild, James Ferryman, Fernando Alonso-Fernandez, Kiran B. Raja, R. Raghavendra, Christoph Busch, and Joseph Bigun. Cross-Eyed - Cross-Spectral Iris/Periocular Recognition Database and Competition. In *2016 International Conference of the Biometrics Special Interest Group (BIOSIG)*, volume P-260, pages 1–5. IEEE, sep 2016.
- [49] Maria De Marsico, Michele Nappi, Daniel Riccio, and Harry Wechsler. Mobile Iris Challenge Evaluation (MICHE)-I, biometric iris dataset and protocols. *Pattern Recognition Letters*, 57:17–23, 2015.
- [50] Ana Sequeira, João Monteiro, Ana Rebelo, and Helder Oliveira. Mobbio: a multimodal database captured with a portable handheld device. volume 3, 01 2014.
- [51] Zijng Zhao and Ajay Kumar. A deep learning based unified framework to detect, segment and recognize irises using spatially corresponding features. *Pattern Recognition*, 93:546–557, sep 2019.

- [52] Caiyong Wang, Yunlong Wang, Yunfan Liu, Zhaofeng He, Ran He, and Zhenjun Sun. Sclerasetnet: An attention assisted u-net model for accurate sclera segmentation. *IEEE Transactions on Biometrics, Behavior, and Identity Science*, PP:1–1, 12 2019.
- [53] Ian Goodfellow, Jean Pouget-Abadie, Mehdi Mirza, Bing Xu, David Warde-Farley, Sherjil Ozair, Aaron Courville, and Yoshua Bengio. Generative adversarial nets. In *NIPS*, pages 2672–2680. Curran Associates, Inc., 2014.
- [54] J. Long, E. Shelhamer, and T. Darrell. Fully convolutional networks for semantic segmentation. In *2015 IEEE Conference on Computer Vision and Pattern Recognition (CVPR)*, pages 3431–3440, June 2015.
- [55] S. Kumar and M. Hebert. A hierarchical field framework for unified context-based classification. In *Tenth IEEE International Conference on Computer Vision (ICCV’05) Volume 1*, volume 2, pages 1284–1291 Vol. 2, Oct 2005.
- [56] Derek Hoiem, Alexei A. Efros, and Martial Hebert. Putting objects in perspective. *International Journal of Computer Vision*, 80(1):3–15, Oct 2008.
- [57] Z. Tu and X. Bai. Auto-context and its application to high-level vision tasks and 3d brain image segmentation. *IEEE Transactions on Pattern Analysis and Machine Intelligence*, 32(10):1744–1757, Oct 2010.
- [58] Antonio Torralba. Contextual priming for object detection. *International Journal of Computer Vision*, 53(2):169–191, Jul 2003.
- [59] Michael Fink and Pietro Perona. Mutual boosting for contextual inference. In *Proceedings of the 16th International Conference on Neural Information Processing Systems, NIPS’03*, pages 1515–1522, Cambridge, MA, USA, 2003. MIT Press.
- [60] Peter Carbonetto, Nando De Freitas, and Kobus Barnard. A statistical model for general contextual object recognition. In *European conference on computer vision*, pages 350–362. Springer, 2004.
- [61] Xuming He, Richard S. Zemel, and Miguel Á. Carreira-Perpiñán. Multiscale conditional random fields for image labeling. In *Proceedings of the 2004 IEEE Computer Society Conference on Computer Vision and Pattern Recognition, CVPR’04*, pages 695–703, Washington, DC, USA, 2004. IEEE Computer Society.
- [62] A. Rabinovich, A. Vedaldi, C. Galleguillos, E. Wiewiora, and S. Belongie. Objects in context. In *2007 IEEE 11th International Conference on Computer Vision*, pages 1–8, Oct 2007.
- [63] C. Galleguillos, A. Rabinovich, and S. Belongie. Object categorization using co-occurrence, location and appearance. In *2008 IEEE Conference on Computer Vision and Pattern Recognition*, pages 1–8, June 2008.
- [64] Lior Wolf and Stanley Bileschi. A critical view of context. *International Journal of Computer Vision*, 69(2):251–261, Aug 2006.
- [65] Jakob Verbeek and Bill Triggs. Scene segmentation with conditional random fields learned from partially labeled images. In *Proceedings of the 20th International Conference on Neural Information Processing Systems, NIPS’07*, pages 1553–1560, USA, 2007. Curran Associates Inc.
- [66] M. Everingham, L. Van Gool, C. K. I. Williams, J. Winn, and A. Zisserman. The PASCAL Visual Object Classes Challenge 2007 (VOC2007) Results, 2007.
- [67] Microsoft Corporation. Microsoft research cambridge (msrc). <https://www.microsoft.com/en-us/download/details.aspx?id=52644>, 2005.
- [68] Sanjiv Kumar, Alexander C Loui, and Martial Hebert. An observation-constrained generative approach for probabilistic classification of image regions. *Image and Vision Computing*, 21(1):87–97, 2003.
- [69] Antonio Torralba, Kevin P. Murphy, and William T. Freeman. Contextual models for object detection using boosted random fields. In *Proceedings of the 17th International Conference on Neural Information Processing Systems, NIPS’04*, pages 1401–1408, Cambridge, MA, USA, 2004. MIT Press.
- [70] J. Leng, Y. Liu, T. Zhang, and P. Quan. Context learning network for object detection. In *2018 IEEE International Conference on Data Mining Workshops (ICDMW)*, pages 667–673, Nov 2018.
- [71] J. Leng, Y. Liu, T. Zhang, P. Quan, and Z. Cui. Context-aware u-net for biomedical image segmentation. In *2018 IEEE International Conference on Bioinformatics and Biomedicine (BIBM)*, pages 2535–2538, Dec 2018.
- [72] Hang Zhang, Jia Xue, and Kristin Dana. Deep ten: Texture encoding network. In *Proceedings of the IEEE Conference on Computer Vision and Pattern Recognition*, pages 708–717, 2017.
- [73] M. Marsico, M. Nappi, D. Riccio, and H. Wechsler. Mobile iris challenge evaluation (MICHE)-I, biometric iris dataset and protocols. *Pattern Recognition Letters*, 57:17–23, 2015.
- [74] Frank Wilcoxon, SK Katti, and Roberta A Wilcox. Critical values and probability levels for the wilcoxon rank sum test and the wilcoxon signed rank test. *Selected tables in mathematical statistics*, 1:171–259, 1970.

- [75] Marvin Teichmann, Michael Weber, J. Marius Zöllner, Roberto Cipolla, and Raquel Urtasun. Multinet: Real-time joint semantic reasoning for autonomous driving. *CoRR*, abs/1612.07695, 2016.
- [76] Phillip Isola, Jun-Yan Zhu, Tinghui Zhou, and Alexei A. Efros. Image-to-image translation with conditional adversarial networks. *CoRR*, abs/1611.07004, 2016.

Tabela 4: Performance comparison among the baseline approaches and the proposed ORCNet approach employing the MICHE-I dataset as input data. Intersection over Union (IoU) is considered as the prior measure ranking methods.

Dataset	Approach	RoI	F-Score	ER	IoU	
MICHE-GS4	EncNet ResNet-50	ALL	93.77 ± 5.31	0.34 ± 0.22	86.31 ± 11.81	
	EncNet ResNet-101		93.40 ± 5.41	0.40 ± 0.24	83.80 ± 13.41	
	EncNet ResNet-152		93.51 ± 4.95	0.37 ± 0.21	85.17 ± 12.82	
	FCN		78.60 ± 13.19	1.22 ± 0.92	66.38 ± 15.36	
	GAN		92.99 ± 7.20	0.37 ± 0.23	87.51 ± 9.75	
	GAN PROCESSED		93.60 ± 6.13	0.34 ± 0.22	88.39 ± 8.53	
	ORCNet ResNet-50		94.65 ± 3.65	0.28 ± 0.17	88.77 ± 9.26	
	ORCNet ResNet-101		94.78 ± 3.47	0.28 ± 0.16	89.31 ± 7.47	
	ORCNet ResNet-152		95.09 ± 3.32	0.27 ± 0.16	89.91 ± 6.90	
	EncNet ResNet-50		Iris	94.67 ± 3.70	0.18 ± 0.13	88.36 ± 11.65
	EncNet ResNet-101	94.15 ± 4.82		0.20 ± 0.13	86.79 ± 13.04	
	EncNet ResNet-152	94.66 ± 3.57		0.19 ± 0.13	87.51 ± 11.84	
	FCN	69.10 ± 15.67		0.73 ± 0.55	52.98 ± 16.50	
	GAN	80.12 ± 11.90		0.51 ± 0.25	68.13 ± 13.31	
	GAN PROCESSED	82.34 ± 11.52		0.42 ± 0.22	71.25 ± 13.15	
	ORCNet ResNet-50	94.81 ± 3.28		0.16 ± 0.11	89.39 ± 9.53	
	ORCNet ResNet-101	94.98 ± 4.08		0.16 ± 0.10	89.98 ± 8.15	
	ORCNet ResNet-152	95.33 ± 2.73		0.15 ± 0.09	90.62 ± 7.58	
	EncNet ResNet-50	Sclera		85.52 ± 8.91	0.30 ± 0.21	73.09 ± 15.23
	EncNet ResNet-101		83.67 ± 9.64	0.33 ± 0.21	69.70 ± 16.80	
	EncNet ResNet-152		85.17 ± 9.53	0.32 ± 0.19	70.90 ± 17.86	
	FCN		69.10 ± 15.67	0.73 ± 0.55	52.98 ± 16.50	
	GAN		80.12 ± 11.90	0.51 ± 0.25	68.13 ± 13.31	
	GAN PROCESSED		82.34 ± 11.52	0.42 ± 0.22	71.25 ± 13.15	
	ORCNet ResNet-50		88.27 ± 6.75	0.25 ± 0.16	78.42 ± 11.60	
	ORCNet ResNet-101		88.44 ± 5.77	0.25 ± 0.17	79.02 ± 9.81	
	ORCNet ResNet-152		88.57 ± 5.60	0.24 ± 0.17	79.51 ± 9.41	
	MICHE-GT2		EncNet ResNet-50	ALL	93.57 ± 5.63	0.57 ± 0.39
		EncNet ResNet-101	94.03 ± 6.34		0.51 ± 0.39	85.38 ± 15.97
		EncNet ResNet-152	94.01 ± 5.83		0.54 ± 0.46	84.75 ± 16.98
		FCN	89.56 ± 7.41		0.96 ± 1.04	81.02 ± 12.84
		GAN	86.31 ± 10.80		1.12 ± 0.68	76.72 ± 13.51
		GAN PROCESSED	88.25 ± 13.19		0.90 ± 0.65	80.31 ± 15.71
		ORCNet ResNet-50	95.19 ± 4.76		0.35 ± 0.25	89.92 ± 11.32
		ORCNet ResNet-101	95.40 ± 4.65		0.34 ± 0.25	90.30 ± 11.52
		ORCNet ResNet-152	95.38 ± 4.92		0.34 ± 0.27	90.37 ± 11.32
EncNet ResNet-50		Iris	94.17 ± 6.85		0.28 ± 0.24	86.55 ± 16.76
EncNet ResNet-101			94.84 ± 5.86	0.26 ± 0.25	87.39 ± 17.10	
EncNet ResNet-152			94.79 ± 6.09	0.27 ± 0.26	87.10 ± 18.08	
FCN			89.93 ± 7.08	0.56 ± 0.52	80.80 ± 14.41	
GAN			91.40 ± 9.59	0.44 ± 0.41	82.92 ± 17.39	
GAN PROCESSED			91.27 ± 10.32	0.45 ± 0.43	82.45 ± 18.63	
ORCNet ResNet-50			95.50 ± 4.68	0.21 ± 0.21	90.14 ± 13.54	
ORCNet ResNet-101			95.75 ± 5.27	0.20 ± 0.25	90.56 ± 13.92	
ORCNet ResNet-152			95.96 ± 4.86	0.19 ± 0.20	90.75 ± 13.74	
EncNet ResNet-50				83.04 ± 13.10	0.48 ± 0.31	68.98 ± 18.46
EncNet ResNet-101		84.67 ± 12.04		0.45 ± 0.30	71.40 ± 18.43	
EncNet ResNet-152		83.81 ± 13.03		0.47 ± 0.37	70.37 ± 19.44	